

Broadband Local Wavenumber Estimation for Damage Detection and Quantification in CFRP Components

Joost SEGERS ¹, Saeid HEDAYATRASAE ^{1,2}, Gaétan POELMAN ¹, Wim VAN PAEPEGEM ¹,
Mathias KERSEMANS ^{1*}

¹ Mechanics of Materials and Structures (UGent-MMS), Department of Materials, Textiles and Chemical Engineering (MaTCh), Ghent University, Technologiepark-Zwijnaarde 46, 9052 Zwijnaarde, Belgium

² SIM Program M3 DETECT-IV, Technologiepark-Zwijnaarde 48, B-9052 Zwijnaarde, Belgium

*Corresponding author: Mathias.Kerseman@Ugent.be

Abstract

Local wavenumber estimation (LWE) is traditionally applied to a narrowband full wavefield response of the test specimen. The technique proves promising for damage detection in fiber-reinforced polymer (i.e. composite) structures. However, the narrowband nature of the traditional LWE techniques bring several challenges for application on actual test cases.

In this paper, the performance of a novel self-reference broadband version of the LWE technique is investigated. The technique is based on modepass filters in the wavenumber-frequency domain. Compared to the traditional narrowband LWE implementations, the proposed method allows a higher level of automation, removes the need for a priori knowledge on the material and/or defect properties, and results in an improved characterization of defects. The performance is evaluated for an aluminum plate with flat bottom hole defects and for a damaged cross-ply CFRP aircraft panel.

Keywords: Fiber-reinforced polymers, Composites; Non-destructive testing (NDT), Self-reference Broadband Local Wavenumber Estimation, Scanning laser Doppler vibrometry, Guided Waves, Depth quantification

1. Introduction

Composite materials (e.g. carbon fiber-reinforced polymers CFRP) are increasingly used for critical components in several industrial sectors (for example aerospace, automotive). A major challenge is the detection of internal damages in these composites which may have occurred during manufacturing or during operational life. One possibility for damage detection in thin-walled composite structures is to analyze the vibrational response measured on the surface. Many different wave actuation and sensing configurations are possible, combined with advanced data processing methods. In this study, piezoelectric actuators are used for excitation combined with a 3D scanning laser Doppler vibrometer (SLDV) to measure the resulting full wavefield.

In the last decades, multiple methods were developed to convert the full wavefield dataset to a damage map [1-13]. Among others, local wavenumber estimation (LWE) has gained a lot of attention as it seems promising for accurate defect detection and quantification. As the name indicates, the wavenumber of a specific Lamb mode is estimated at each point of the component. For linear isotropic materials, the Rayleigh-Lamb equation (also referred to as the dispersion relation) gives the relation between the local wavenumber k [1/m], the temporal frequency of the wave f [Hz] and the local material thickness d [m] [14]:

$$\frac{\tanh\left(\frac{\beta d}{2}\right)}{\tanh\left(\frac{\alpha d}{2}\right)} = \left[\frac{((2\pi k)^2 + \beta^2)^2}{4\alpha\beta(2\pi k)^2} \right]^s \quad \text{with} \quad \begin{aligned} \alpha^2 &= (2\pi)^2 \left(k^2 - \frac{f^2}{c_l^2} \right) \\ \beta^2 &= (2\pi)^2 \left(k^2 - \frac{f^2}{c_t^2} \right) \end{aligned} \quad (1)$$

Where c_l and c_t are the material's longitudinal and transverse wave velocity, respectively. The parameter s equals +1 or -1 for the anti-symmetric or symmetric Lamb modes, respectively. As an example, the dispersion curves of (isotropic) aluminum ($c_l = 6420$ m/s, $c_t = 3040$ m/s) are shown in Figure 1. In Figure 1 (a), the solution is given in terms of the wavenumber-thickness product versus the frequency-thickness product, resulting in a single dispersion curve that is valid for any material thickness d . In Figure 1 (b), the dispersion curves are shown for an aluminum plate of specified thicknesses. Note that for the A_0 mode, the wavenumber increases when the material thickness becomes smaller. As such, a horizontal crack in the aluminum plate will result in the local increase of the A_0 mode wavenumber as graphically illustrated on Figure 1 (c). In the same way, a delamination defect in a composite plate results in an increased local wavenumber for the A_0 mode.

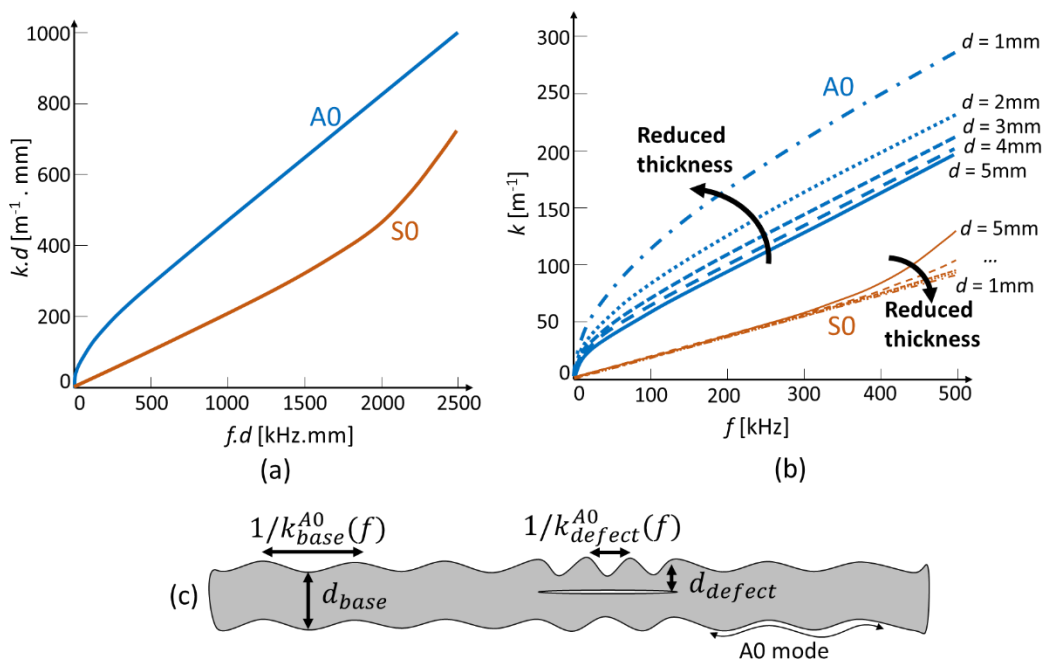


Figure 1: Dispersion characteristics of aluminum material: (a) Dispersion curves expressed as wavenumber-thickness $k \cdot d$ in function of frequency-thickness $f \cdot d$, (b) Dispersion curves expressed as wavenumber k in function of frequency f for several material thicknesses d and (c) Schematic illustration of the local change in A_0 mode dispersion behavior at a horizontal crack or delamination.

Multiple LWE algorithms were developed, also resulting in a multitude of other names for LWE such as, acoustic wavenumber spectroscopy, instantaneous wavenumber estimation, multi-frequency LWE, etc [15-19]. All the mentioned LWE approaches have in common that the wavenumber map is obtained corresponding to a specific (center) frequency of excitation and a specific Lamb mode. In

most cases, the A_0 mode is chosen because the A_0 mode dispersion curve varies in function of the material's thickness d over the complete frequency axis (see Figure 1 (b)).

Recently, a novel LWE approach is proposed by the current authors which considers broadband excitation and subsequent self-reference mode filtering in the wavenumber-frequency domain [20]. The broadband response of the test specimen is obtained using sine sweep piezoelectric excitation (or pulsed laser excitation), combined with SLDV measurements. The novel self-reference broadband local wavenumber estimation (SRB-LWE) approach shows an enhanced performance on the level of defect evaluation and reduction of the required user input compared to the traditional LWE implementations. A local thickness map is obtained while the only parameter that needs to be known in advance is the base material thickness (or most prominent thickness) of the investigated test specimen. And even in case that also this thickness is unknown, the SRB-LWE will give the relative local thickness compared to the base material.

In this paper, the performance of SRB-LWE is further investigated. First, the measurement procedure and the used test specimens are described. Next, the defect detection and depth identification capability of SRB-LWE is evaluated for a 5 mm thick aluminum plate with flat bottom hole defects and for a 1.1 mm thick CFRP aircraft panel with a disbanded backside stiffener.

2. Materials and Measurements

SRB-LWE is performed on two test specimens (see Figure 2).

The first test specimens is a 400x400x5 mm³ aluminum plate. Ten flat bottom holes (FBHs) with diameter \varnothing 25 mm are milled into the backside of the plate. Figure 2 (a) shows the plate together with a table wherein the remaining material thickness d of every FBH is specified. Note that there is one FBH with a remaining thickness of 0 mm that is thus an open hole.

The second component is a CFRP part manufactured for use in the vertical stabilizer of an Airbus A320 aircraft (see Figure 2 (b)). On the backside, stiffeners are visible which are bonded to a base plate. The thickness of the base plate, on which the stiffeners are bonded, measures 1.1 mm. The component is manufactured using a cross-ply layup. The material's elastic properties and densities are unknown. The component was scrapped by the manufacturer because an ultrasonic C-scan inspection revealed a defect at the central stiffener. The time-of-flight (TOF) map obtained from in-house immersion ultrasonic C-scan inspection using a 5 MHz focused transducer in reflection mode is added to the figure. This C-scan result reveals a relatively large disbond between the central stiffener and the base plate.

Vibrations are introduced through small, low power piezoelectric actuators (Ekulit type EPZ-20MS64W). The actuators are attached to the backside using phenyl salicylate which has the advantage that the actuators can be easily removed by re-melting (> 41 °C) this bonding substance. A broadband sine sweep voltage signal is generated using the SLDV's built-in function generator. The sweep's start and end frequencies are listed in Table 1. The voltage signal is amplified through a Falco WMA-300 high voltage amplifier before it is supplied to the piezoelectric actuator.

The full wavefield velocity response is recorded using a 3D infrared SLDV (Polytec PSV-500 3D Xtra). For each test specimen, the area for which the wavefield is recorded (i.e. scan area) is indicated on Figure 2. All relevant data acquisition settings, i.e. sampling frequency f_s , number of samples, number of averages and scan point spacing are included in Table 1. Only the out-of-plane velocity component $V_z(x, y, t)$ is used because the SRB-LWE algorithm is operated on the A_0 Lamb mode, which has a dominant out-of-plane surface vibration.

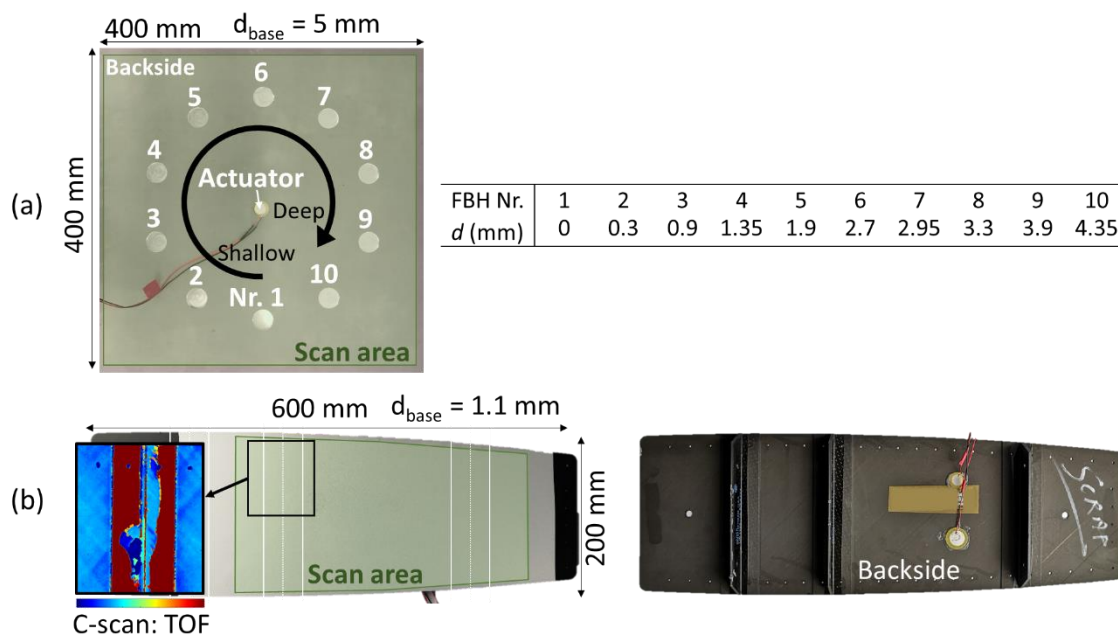


Figure 2: Test specimen: (a) Aluminum plate with 10 flat bottom holes of diameter 25 mm and remaining material thickness d , (b) CFRP aircraft panel with disbond at the central stiffener.

Table 1: Characteristics of excitation signals and SLDV data acquisition.

Material	Defect	Excitation			SLDV			
		f_{start} (kHz)	f_{end} (kHz)	V_{pp}	f_s (kS/s)	# samples	# averages	point spacing (mm)
Al 5 mm	FBH Ø 25 mm	5	300	100	1250	10 000	20	3
CFRP 1.1 mm + Stiffeners	Disbond	5	300	50	625	10 000	15	2

3. Self-reference Broadband Local Wavenumber Estimation Algorithm

The SRB-LWE algorithm consists of multiple signal processing steps which are discussed in detail by the current authors in Ref. [20]. A short summary is provided below.

First, the dispersion curves correspond to the damage-free material are identified in the broadband response of the component. The vibrations that are related to modes different from the A_0 mode (i.e. the S_0 mode vibrations) are removed using a modestop filter.

Next, the broadband response is ran through a bank of A_0 modepass filters. Each modepass filter assumes a certain material thickness. The filters are calculated solely based on the identified dispersion curve that corresponds to the damage-free material (i.e. self-reference approach). The bandwidth of the filters is automatically determined.

At last, the local material thickness is identified by looking at the broadband energy (i.e. bandpower) in the modepass filtered velocity fields. The defects are readily identified as local anomalies in the material's thickness.

4. SRB-LWE Results and Discussion

4.1 Aluminum Plate with FBHs

SRB-LWE is performed for the measurement results of the 5 mm thick aluminum plate that contains FBH defects of diameter 25 mm and variable remaining material thickness d (see also Figure 2 (a)). The resulting estimated local thickness map is shown in Figure 3 (a). Figure 3 (b) shows line plots of the estimated local thickness at the location of each FBH defect. The true defect diameter (i.e. 25 mm) and the true remaining thicknesses d are indicated on these graphs using dashed lines. In addition, the estimated and true local thickness at each FBH are listed in Figure 3 (c).

The estimated local thickness map is of high quality and reveals all defects, including shallow defects as well as deep defects with a depth higher than 80% of the base material's thickness. In general, the estimated thickness is in good agreement with the true remaining material thickness as seen in Figure 3 (b) and (c). Note that the thickness is estimated with a resolution of 0.2 mm [20].

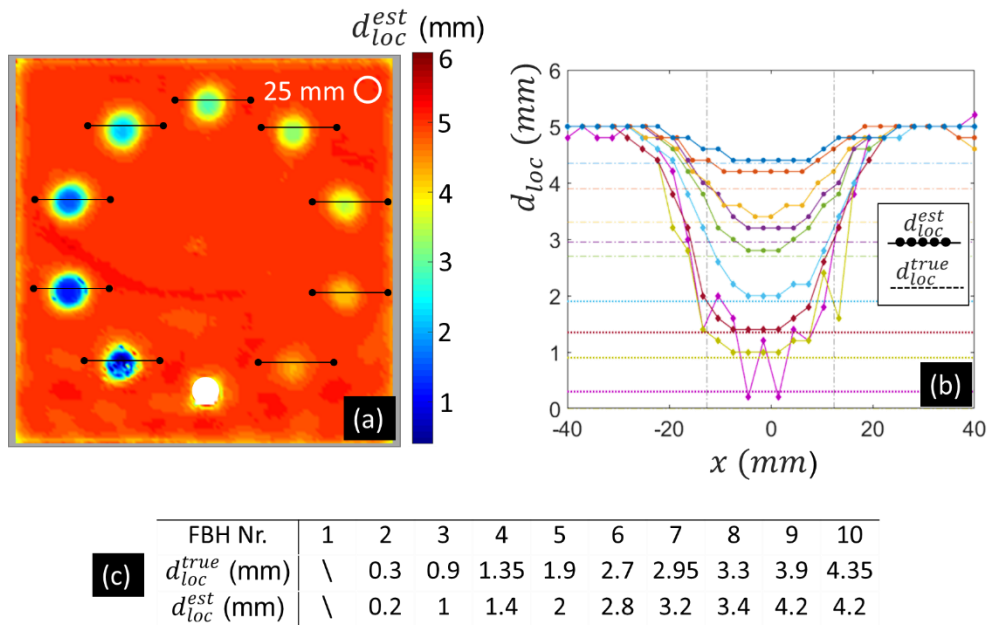


Figure 3: Results from SRB-LWE for aluminum plate with FBHs of variable remaining material thickness d , (a) Estimated local thickness map, (b) Estimated local thickness at line through the FBHs and (c) True and estimated local thickness at the FBHs.

4.2 CFRP Aircraft Panel with Disbond

The aircraft panel was manufactured by an industrial partner, and the disbond was unintentionally generated during the manufacturing process. The global wavenumber-frequency map (along $k_y = 0$ m^{-1}) of the measurement is displayed in Figure 4 (a), and the identified dispersion curves of the A_0 and S_0 modes are shown on top with white lines.

Figure 4 (b) shows the TOF map derived from the ultrasonic C-scan inspection. The disbond at the stiffener is revealed by the reduced TOF value. Note that the thickening at the stiffener's middle fin (see also Figure 2 (b)) is not found using the TOF C-scan results.

Figure 4 (c) represents the estimated local thickness map obtained from the proposed SRB-LWE algorithm. For comparison, Figure 4 (d) shows the local wavenumber map obtained from the traditional LWE implementation proposed by Flynn et al. [15]. For this traditional LWE algorithm, a 5-cycle Hanning windowed sine excitation with center frequency 150 kHz was employed, and the algorithm's parameters were selected through trial and error.

The estimated local thickness map obtained through the proposed SRB-LWE algorithm correctly shows the extent of the disbond, i.e. where a local thickness is found similar to the thickness of the base material, i.e. 1.1 mm. A significant improvement in damage identification and evaluation is observed when comparing this local thickness map to the local wavenumber map obtained from traditional LWE. The improved quality is caused by the superior filter efficiency of using a mode filter

(instead of a wavenumber filter), by the averaging effect of employing a broadband approach, by the use of a SNR criterion for frequency frame selection and by the self-reference thickness estimation (rather than wavenumber estimation) [20]. Because of this high-quality output of SRB-LWE, it is even possible to estimate the local thickness at the non-defected stiffener's area. The found value of $d_{loc}^{est} = 2.20$ mm matches perfectly with the true local thickness $d_{loc}^{true} = 2.18$ mm.

One may notice small discrepancies in the estimated local thickness maps that are caused by the non-isotropy of the composite material [20]. In between the two stiffeners, the true local thickness is 1.1 mm. However, the estimated local thickness map shows a small increase in estimated thickness in the -45° direction around the piezoelectric actuator (see Figure 4 (c)). This local thickness increase must be linked to the layup of the laminate. Therefore, it is expected that the outer plies, which contribute most to the flexural rigidity, have a -45° angle. This expected layup is confirmed after consulting the manufacturer of the aircraft component, who specifies a $[(-45^\circ/+45^\circ)]_2s$ layup for the studied component.

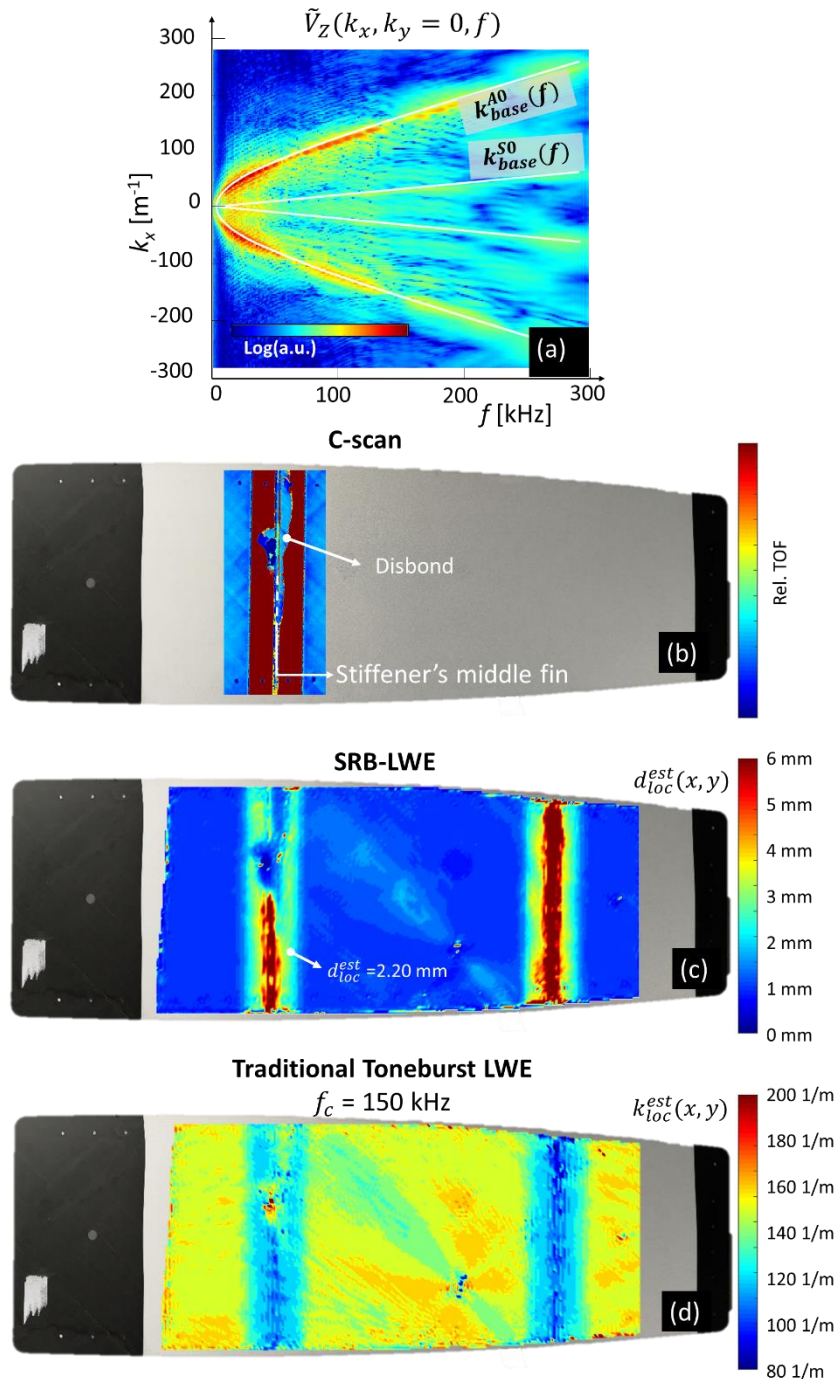


Figure 4: Aircraft CFRP component with disbond at stiffener: (a) Wavenumber-frequency map for the out-of-plane velocity response along $k_y = 0$, together with the identified A_0 and S_0 mode curves, (b) C-scan time-of-flight map at damaged stiffener, (c) SRB-LWE derived thickness map, (d) Traditional LWE [15] derived wavenumber map.

5. Conclusion

The novel full wavefield inspection method: “Self-reference broadband local wavenumber estimation (SRB-LWE)” is used for damage detection in composite components. The procedure results in an estimated local thickness map of the inspected area, in which defects are found as areas of abnormal local thickness. The SRB-LWE algorithm is baseline-free, user-independent and does not require the elastic material properties to be known.

Broadband vibrations are introduced in the component using low-power piezoelectric actuators. A scanning laser Doppler vibrometer records the full wavefield response. The A_0 mode is chosen as the mode of interest for SRB-LWE.

The high performance of the SRB-LWE algorithm is verified for an aluminum plate with flat bottom hole defects, and for a cross-ply CFRP aircraft panel with disbanded backside stiffener. The estimated local thickness maps are found to not only reveal the extent of the defects with high precision, but to also give accurate depth estimation of the defects.

Acknowledgements

The authors acknowledge Fonds voor Wetenschappelijk Onderzoek FWO (grant number 1148018N), Bijzonder Onderzoeks Fonds BOF (grant number 01N01719) and the SBO project DETECT-IV (Grant no. 160455), which fits in the SIM research program MacroModelMat (M3) coordinated by Siemens (Siemens Digital Industries Software, Belgium) and funded by SIM (Strategic Initiative Materials in Flanders) and VLAIO (Flemish government agency Flanders Innovation & Entrepreneurship). The authors further thank SABCA Limburg for providing the CFRP aircraft panels.

References

1. Ostachowicz, W., M. Radziński, and P. Kudela, *50th Anniversary Article: Comparison Studies of Full Wavefield Signal Processing for Crack Detection*. Strain, 2014. **50**(4): p. 275-291.
2. Segers, J., et al., *Backside delamination detection in composites through local defect resonance induced nonlinear source behaviour*. Journal of Sound and Vibration, 2020. **479**.
3. Segers, J., et al., *Nonlinear Elastic Wave Energy Imaging for the Detection and Localization of In-Sight and Out-of-Sight Defects in Composites*. Applied Sciences, 2020. **10**(3924).
4. Segers, J., et al., *Robust and baseline-free full-field defect detection in complex composite parts through weighted broadband energy mapping of mode-removed guided waves*. Mechanical Systems and Signal Processing, 2021. **151**.
5. Radziński, M., et al., *Damage Identification in Various Types of Composite Plates Using Guided Waves Excited by a Piezoelectric Transducer and Measured by a Laser Vibrometer*. Sensors (Basel, Switzerland), 2019. **19**(9).
6. Keshmiri Esfandabadi, Y., et al., *Full Wavefield Analysis and Damage Imaging Through Compressive Sensing in Lamb Wave Inspections*. IEEE transactions on ultrasonics, ferroelectrics, and frequency control, 2018. **65**(2): p. 269-280.
7. Cuomo, S., et al., *Machine learning for impact detection on composite structures*. Materials Today: Proceedings, 2020.

8. Song, H. and Y. Yang, *Super-resolution visualization of subwavelength defects via deep learning-enhanced ultrasonic beamforming: A proof-of-principle study*. NDT & E International, 2020. **116**.
9. Spytek, J., et al., *Multi-resolution non-contact damage detection in complex-shaped composite laminates using ultrasound*. NDT & E International, 2020. **116**.
10. Sha, G., et al., *Guided wavefield curvature imaging of invisible damage in composite structures*. Mechanical Systems and Signal Processing, 2021. **150**.
11. Wu, Z., S.Y. Chong, and M.D. Todd, *Laser ultrasonic imaging of wavefield spatial gradients for damage detection*. Structural Health Monitoring, 2020.
12. Kudela, P., M. Radziński, and W. Ostachowicz, *Identification of cracks in thin-walled structures by means of wavenumber filtering*. Mechanical Systems and Signal Processing, 2015. **50-51**: p. 456-466.
13. Kudela, P., M. Radziński, and W. Ostachowicz, *Impact induced damage assessment by means of Lamb wave image processing*. Mechanical Systems and Signal Processing, 2018. **102**: p. 23-36.
14. Rose, J.L., *Ultrasonic Guided Waves in Solid Media*. 2014: Cambridge University Press.
15. Flynn, E.B., et al., *Structural imaging through local wavenumber estimation of guided waves*. NDT & E International, 2013. **59**: p. 1-10.
16. Rogge, M.D. and C.A. Leckey, *Characterization of impact damage in composite laminates using guided wavefield imaging and local wavenumber domain analysis*. Ultrasonics, 2013. **53(7)**: p. 1217-26.
17. Jeon, J.Y., et al., *2D-wavelet wavenumber filtering for structural damage detection using full steady-state wavefield laser scanning*. NDT & E International, 2020. **116**.
18. Jeon, J.Y., et al., *Damage detection on composite structures with standing wave excitation and wavenumber analysis*. Advanced Composite Materials, 2017. **26(sup1)**: p. 53-65.
19. Mesnil, O., C.A.C. Leckey, and M. Ruzzene, *Instantaneous and local wavenumber estimations for damage quantification in composites*. Structural Health Monitoring, 2014. **14(3)**: p. 193-204.
20. Segers, J., et al., *Self-Reference Broadband Local Wavenumber Estimation (SRB-LWE) for defect assessment in composites* Mechanical Systems and Signal Processing, 2021. **163**.